



Universidad Autónoma  
de Madrid

**Biblos-e Archivo**  
Repositorio Institucional UAM

**Repositorio Institucional de la Universidad Autónoma de Madrid**

<https://repositorio.uam.es>

Esta es la **versión de autor** del artículo publicado en:  
This is an **author produced version** of a paper published in:

Fuel 305 (2021): 121506

**DOI:** <https://doi.org/10.1016/j.fuel.2021.121506>

**Copyright:** © 2021 Elsevier Ltd. This manuscript version is made available under the CC-BY-NC-ND 4.0 licence <http://creativecommons.org/licenses/by-nc-nd/4.0/>

El acceso a la versión del editor puede requerir la suscripción del recurso  
Access to the published version may require subscription

# Continuous aqueous phase reforming of wastewater streams: A catalyst deactivation study

A.S. Oliveira<sup>1</sup>, T. Cordero-Lanzac<sup>2</sup>, J.A. Baeza<sup>1</sup>, L. Calvo<sup>1\*</sup>, J.J. Rodriguez<sup>1</sup>, M.A. Gilarranz<sup>1</sup>

<sup>1</sup> Department of Chemical Engineering, Universidad Autónoma de Madrid, 28049 Madrid, Spain

<sup>2</sup> Department of Chemical Engineering, University of the Basque Country, 48080, Bilbao, Spain

\*corresponding author e-mail: luisa.calvo@uam.es

## Abstract

This paper reports on the catalytic performance and deactivation in aqueous phase reforming of wastewater streams for H<sub>2</sub> production. Brewery wastewater was chosen as representative of this type of effluent. The effect of catalyst support textural characteristics was evaluated using an activated carbon and different modified supports obtained by infiltration and carbonization of a phenolic resol resin into activated carbon. The effect of active phase was evaluated using Pt and PtRe catalysts with different metal molar ratio. At short time on stream values, Pt catalysts supported on modified activated carbon showed higher H<sub>2</sub> production than those supported on unmodified activated carbon, indicating that a lower microporosity facilitates the transport of reactants to catalytic active sites and release of reaction products. Bimetallic PtRe catalysts showed higher activity than Pt, particularly using a metal molar ratio of 1:1, which yielded the highest H<sub>2</sub> production (117.2  $\mu\text{mol min}^{-1}$ ). Despite the different catalysts tested, early and significant deactivation was observed. The characterization of used catalysts allows postulating the adsorption of organic species and/or coke-like matter deposition on the catalysts surface as main causes of deactivation.

**Keywords:** catalyst deactivation, aqueous phase reforming, brewery wastewater, hydrogen

## 1. Introduction

Hydrogen has been recognized as one of the future energy carriers enabling reduction of greenhouse gas emissions derived from the use of fossil fuels [1–3]. It is a powerful energy alternative cleaner than current fossil fuels, more sustainable for certain applications, and could be a solution for major environmental challenges according to a technical and environmental comparative studies [4]. However, H<sub>2</sub> must be produced from clean and renewable sources to be postulated as an environmentally friendly energy carrier.

H<sub>2</sub> production from aqueous phase reforming (APR) of biomass-derived hydrocarbons has attracted much interest since it was first reported [5], especially because this process has some potential advantages compared to conventional reforming processes such as steam reforming [6]. Among other advantages, the reaction temperatures and pressures generally used in APR process significantly reduce energy consumption, facilitate gas purification, minimize undesirable parallel decomposition reactions, and thermodynamically favour water-gas shift (WGS) reaction, generating H<sub>2</sub> with very low CO content [5,7].

Different supported metal catalysts have been tested in APR. Among them, Pt catalysts are considered as the most effective for H<sub>2</sub> production, since this metal promotes C-C bond cleavage leading to the formation of CO and H<sub>2</sub>, it has an appreciable WGS activity, and minimizes H<sub>2</sub> consumption caused by hydrogenation of intermediates resulting from C-O bond cleavage [8,9]. Some authors have also reported an increase in catalytic activity when a second metal was added to Pt-based catalysts [10–12]. Godina *et al.* [11] have reported that Re addition to Pt catalysts significantly increases the activity in the APR of xylitol, and that the performance shown by the PtRe catalysts is superior to that of other

bimetallic ones such as PtRu, PtNi and PtCo. However, they have also reported lower H<sub>2</sub> selectivity due to reaction shift towards alkanes formation. Ciftci *et al.* [13] have attributed the higher activity of PtRe catalyst in the APR of glycerol to enhanced WGS reaction, although they also pointed out that Re favours dehydration reactions. This route may have an important role in catalytic performance since dehydration of carbohydrates followed by aldol condensation reaction could lead to the formation of coke-precursor species [14,15] that can deactivate the catalyst. Therefore, although the addition of Re increases the catalytic activity of Pt catalysts, more studies are needed to understand its effect on coke formation and deactivation of catalysts in APR.

Regarding the influence of the catalytic support,  $\gamma$ -Al<sub>2</sub>O<sub>3</sub> has been the most frequently support used in APR studies because Pt/ $\gamma$ -Al<sub>2</sub>O<sub>3</sub> catalyst yield high carbon conversion to gas and H<sub>2</sub> selectivity [16–21]. However,  $\gamma$ -Al<sub>2</sub>O<sub>3</sub> is not stable under hydrothermal conditions and undergoes a phase transformation to boehmite [22,23], diminishing catalyst activity [24,25]. On the other hand, carbon supports have been increasingly used due to their stability under APR conditions, tuneable textural and chemical properties, and very high activity of carbon supported catalysts when compared to alumina supported ones [26]. Different types of carbon materials, such as activated carbons [12,27], mesoporous carbons [26,28,29], carbon nanofibers [30] and carbon nanotubes [12,31], have been used as catalysts supports. Furthermore, the textural and surface properties of carbon materials have been claimed as important factors influencing catalyst performance. Kim *et al.* [29] reported higher activity for catalyst based on mesoporous carbons than for those based on activated carbon, which was ascribed to the highly heterogeneous porous texture of activated carbon, with prevailing microporosity that hinders the access of the reactants to the active sites and the diffusion of products towards the gas phase.

Despite the high catalytic activity exhibited by carbon-supported catalysts, deactivation is a challenge for their application in APR, especially when feedstocks containing complex mixtures of organic compounds are used, such as wastewater streams [32]. There are few studies on this topic, as existing literature mostly deals with single model compounds as APR substrates using alumina-supported catalyst. Support structure collapse [25], coking [33,34], metal nanoparticle sintering [35,36], oxidation [37] and leaching of metal active phase [33,38] have been reported as main deactivation causes. Nevertheless, in-depth investigation of carbon-supported catalysts deactivation using complex feedstocks is needed to assess the stability of catalysts in realistic environments and learning on their design and optimization of APR operation conditions.

This work studies the deactivation of Pt and PtRe/C catalysts in the APR in a continuous fixed bed reactor. Brewery wastewater is chosen as representative of feedstocks with complex composition, because it includes sugars, ethanol, proteins from yeast and malt, and volatile fatty acids, among others. With this aim, the influence of catalyst active phase and support characteristics is analysed, using activated carbon-based supports with different textural properties, in an approach not reported before to the best of our knowledge.

## **2. Experimental**

### *2.1. Materials*

Maltose ( $\geq 99\%$ ), malt extract, yeast extract, wheat peptone,  $(\text{NH}_4)_2\text{SO}_4$  ( $\geq 99\%$ ), KOH ( $\geq 99\%$ ),  $\text{H}_2\text{PtCl}_6$  solution (8 wt. % in  $\text{H}_2\text{O}$ ) and  $\text{HReO}_4$  solution (75 – 80 wt. % in  $\text{H}_2\text{O}$ ) were purchased from Sigma-Aldrich. Ethanol ( $\geq 99.5\%$ ) was purchased by Panreac

AppliChem. Commercial activated carbon was supplied by Merck (MER) and phenolic resol resin (PRR) was supplied by Hexion Specialty Chemicals Ibérica, S.A.

## *2.2. Preparation and characterization of supports and catalysts*

Carbon-supported Pt catalysts (3 wt. %) were prepared by incipient wetness impregnation of as received and modified MER activated carbon. Modified activated carbons were prepared by impregnation and further carbonization of PRR (1, 10, 20 and 40 wt. % of MER), with the aim of progressively reducing support microporosity. For impregnation, PRR was dissolved in ethanol, using 0.65 mL of ethanol per g of MER. Carbonization of PRR on impregnated materials was carried out by curing at 130 °C in air during 2 h followed by pyrolysis at 700 °C under N<sub>2</sub> flow during 1 h. As received and modified activated carbon supports were denoted as AC and AC%PRR, respectively, where % corresponds to the mass percentage of PRR used in the impregnation stage. Pt/AC and Pt/AC%PRR catalysts were calcined at 200 °C and reduced at 300 °C under H<sub>2</sub> flow (25 mL per min STP and g of catalyst), both processes during 2 h using a heating rate of 5 °C per min. PtRe/AC (3 wt. % of metal) catalysts, with metal molar ratios of 1:1, 1:2 and 2:1, were prepared by sequential incipient wetness impregnation. These catalysts were calcined at 250 °C for 2 h (heating rate of 5 °C per min) and reduced under the same conditions as the previous catalysts.

The supports and catalysts were characterized by N<sub>2</sub> adsorption-desorption at -196 °C using a TriStar II Micromeritics analyser. Before adsorption measurements, the samples were degassed at 150 °C under a residual pressure of 10<sup>-6</sup> bar for a minimum of 6 h. The specific surface area (S<sub>BET</sub>) was calculated by the BET equation. The external (non-microporous) surface area (A<sub>EXT</sub>) and micropore volume were calculated by t-plot method. Mesopore volume was calculated by BJH method. The acidity of the supports

and catalysts was estimated from the pH slurry, which was determined by measuring the pH of an aqueous suspension consisting of 1 g of the support in 10 mL of distilled water [39]. The surface CHNS-O composition of the catalysts was calculated using a LECO CHNS-932 elementary chemical analyser. The morphology of the catalysts and the size distribution of metal particles were assessed using a JEOL - 3000F scanning transmission electron microscope (STEM). Software 'ImageJ 1.51k' was used for measuring and counting metal nanoparticles (NPs) in digital STEM images. At least 200 NPs per catalyst were used to calculate the mean size and size distribution.

Used catalysts were characterized by temperature-programmed desorption (TG-TPD) and oxidation (TG-TPO) using a TA Instruments Q500 thermogravimetric analyser. During TG-TPD analysis a N<sub>2</sub> flow of 50 mL min<sup>-1</sup> STP was used. Samples were kept heated to 450 °C using a heating rate of 10 °C per min, kept at maximum temperature for 30 min, and then cooled to room temperature. Afterwards, the flow was shifted to air and a TG-TPO was performed at 550 °C during 2 h (heating rate of 5 °C per min).

### *2.3. Preparation and characterization of synthetic brewery wastewater*

Synthetic brewery wastewater (SBW) was prepared according to literature [40] and previous batch APR works [32,41], where behaviour equivalent to that of actual brewery wastewater was confirmed. Brewery wastewater is usually basic due to cleaning-in-place operations commonly used in food and beverage industry. Therefore, KOH was added to adjust the pH of wastewater to 10. SBW was characterized by total organic carbon (TOC), using a TOC-VCSH Shimadzu analyser, and chemical oxygen demand (COD), using a standard method (ASTM D1252). The initial values were around 2000 and 6200 mg L<sup>-1</sup>, for TOC and COD, respectively.

### *2.4. Aqueous phase reforming experiments*

Catalytic performance and stability upon time-on-stream (TOS) were tested in an externally heated continuous fixed bed reactor (stainless steel, 300 x 10 mm i.d.). The reactions conditions were selected in preliminary experiments and based in the results from previous works [42]. Experiments were performed at 225 °C and 28 bar using 1 g of catalyst and a constant Ar carrier gas flow (40 mL min<sup>-1</sup> STP). A PID control system was used to keep the reactor temperature and pressure constant during the experiments. The reaction temperature was monitored using a thermocouple placed in the center of the reactor and on top the catalyst bed. Brewery wastewater was fed into the reactor with a high-performance liquid chromatography (HPLC) pump using a flow rate of 1 mL min<sup>-1</sup>. The unreacted effluent and the gaseous and liquid products were cooled down, depressurized through a back pressure regulation valve (BPR), and discharged to a gas-liquid separator equipped with a hydrostatic pressure differential sensor (HPDS) allowing the control of the liquid level. The liquid phase was discharged through a regulation valve connected to the separator. Gas products leaving the phase separator were analysed online by a gas chromatograph (GC/FID/TCD, 7820A, Agilent) equipped with two packed columns and a molecular sieve. Liquid effluent was characterized by TOC measurements. The experimental set-up is shown in Figure 1.



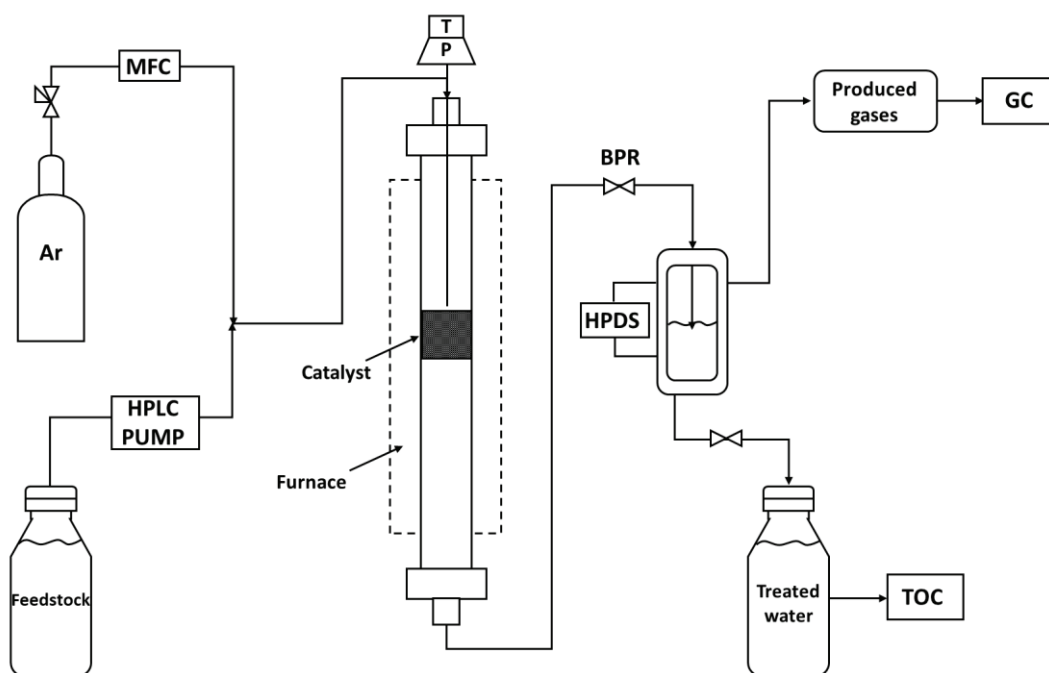


Figure 1. Experimental set-up

TOC removal (%) and carbon conversion to gas (CC gas (%)) were calculated using the following equations:

$$\text{TOC removal (\%)} = \frac{\text{TOC}_{\text{initial}} \text{ (mg/L)} - \text{TOC}_{\text{final}} \text{ (mg/L)}}{\text{TOC}_{\text{initial}} \text{ (mg/L)}} \times 100 \quad (1)$$

$$\text{CC gas (\%)} = \frac{C_{\text{gas}} \text{ (g)}}{C_{\text{initial}} \text{ (g)}} \times 100 \quad (2)$$

Where  $C_{\text{gas}}$  is the C content in the gas products and  $C_{\text{initial}}$  is the initial C content in SBW.

### 3. Results and discussion

#### 3.1. Supports and catalysts characterization

Table 1 shows the porous texture and pH slurry of the supports and catalysts studied. The  $\text{N}_2$  adsorption/desorption isotherms are included as Supplementary Material (Figure S1).

The AC support yielded BET surface area ( $S_{\text{BET}}$ ) and external surface area ( $A_{\text{EXT}}$ ) values typical of an activated carbon with a well-developed porosity, being an essentially microporous solid with significant contribution of mesoporosity. As expected, the microporosity of the AC support was progressively reduced due to impregnation and carbonization of PRR.  $S_{\text{BET}}$ ,  $A_{\text{EXT}}$ , and mesopore volume were also gradually reduced. Despite this, all the modified supports continued to have contribution of microporosity, due to the microporous nature of the char formed from PRR carbonization. Therefore, even in the modified support with 40 wt. % of PRR, the microporosity was not complete eliminated. Pt/AC%PRR catalysts showed a moderate decrease of  $S_{\text{BET}}$ ,  $A_{\text{EXT}}$ , and pore volume respect to the corresponding supports which can be attributed to pore blockage by Pt metallic nanoparticles. The pH slurry of AC was 8.3, increasing after resol resin infiltration, particularly when a higher percentage of PRR was used. PtRe/AC catalysts showed lower  $S_{\text{BET}}$  and pore volume than Pt/AC and markedly lower pH slurry. The increase in surface acidity due to Re addition to Pt/C catalysts was previously reported in literature, although this increase was associated to different species. Zhang *et al.* [43] reported that acidity was due to the existence of Pt–O–Re structures, while King *et al.* [44] related that acidity to ReOx species.

Table 1. Porous texture and pH slurry of supports and catalysts

Samples	$S_{\text{BET}}$ ( $\text{m}^2 \text{g}^{-1}$ )	$A_{\text{EXT}}$ ( $\text{m}^2 \text{g}^{-1}$ )	Micropore volume ( $\text{cm}^3 \text{g}^{-1}$ )	Mesopore volume ( $\text{cm}^3 \text{g}^{-1}$ )	pH slurry
AC	930	120	0.38	0.15	8.3
AC1PRR	870	110	0.37	0.13	8.3
AC10PRR	770	100	0.32	0.12	9.8
AC20PRR	600	80	0.25	0.10	9.8
AC40PRR	490	65	0.20	0.08	9.8
Pt/AC	910	120	0.38	0.14	8.5
Pt/AC1PRR	820	105	0.34	0.12	8.0
Pt/AC10PRR	695	90	0.29	0.11	8.6

Pt/AC20PRR	570	70	0.24	0.09	8.2
Pt/AC40PRR	445	60	0.19	0.06	7.9
1:1PtRe/AC	820	120	0.34	0.15	3.2
1:2PtRe/AC	800	110	0.35	0.13	5.8
2:1PtRe/AC	810	120	0.34	0.14	3.6

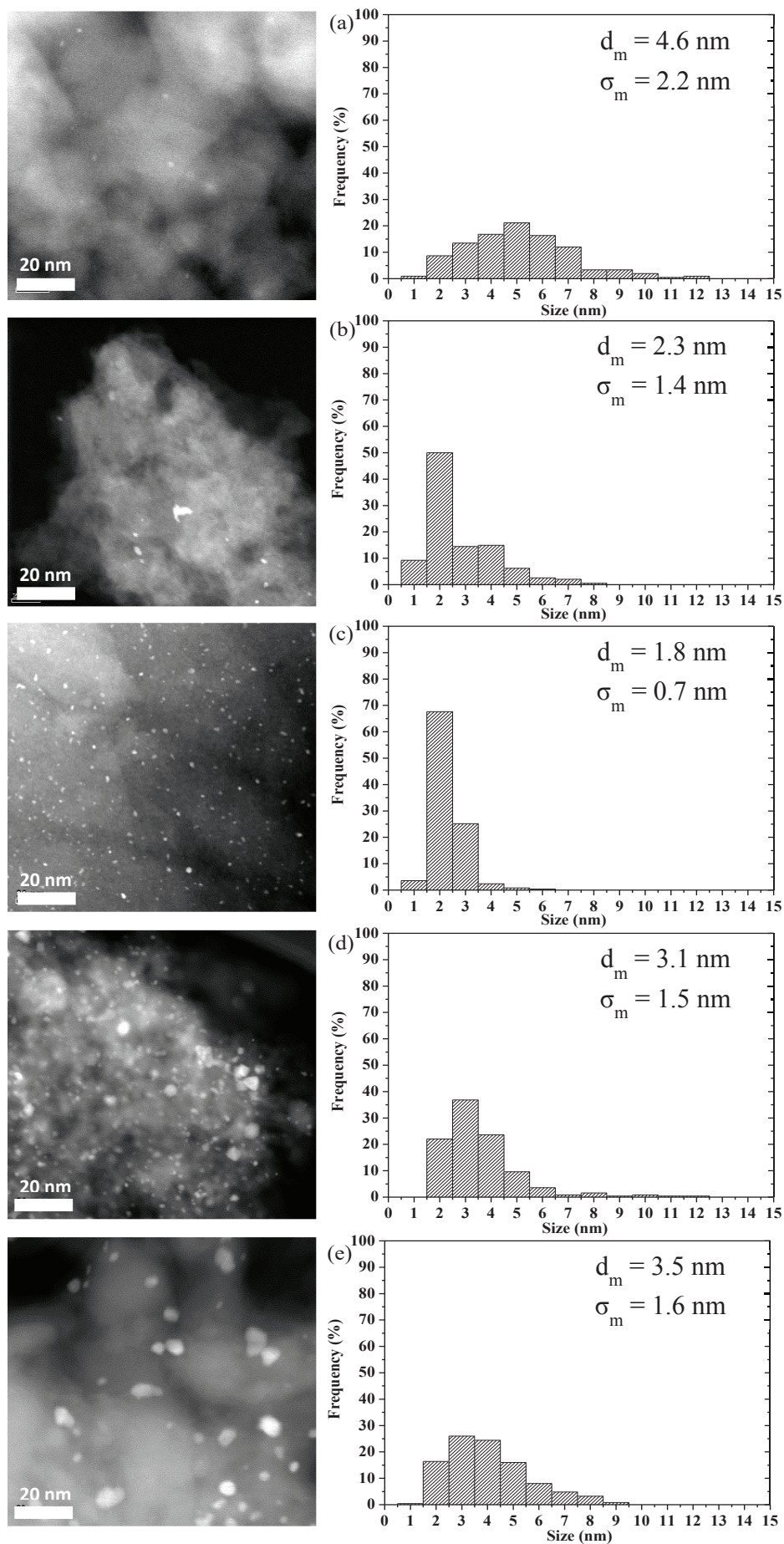
Elemental analysis of carbon-supported Pt catalysts was carried out to evaluate possible changes in the modified supports respect to AC support. As can be observed in Table 2, the percentage of C in the Pt/AC%PRR catalysts slightly changed due to the addition of PRR, although a clear trend was not observed, whereas H percentage gradually increased with PRR addition. Negligible concentrations of N and S was observed in the catalyst, therefore the influence of these heteroatoms on catalytic activity can be ruled out.

Table 2. Elemental composition of Pt/AC and Pt/AC%PRR catalysts

Catalyst	% C	% H	% N	% S	% O <sup>a</sup>
Pt/AC	86.1 ± 0.1	0.4 ± 0.1	0.5 ± 0.1	0.7 ± 0.1	12.3 ± 0.1
Pt/AC1PRR	87.0 ± 0.2	0.4 ± 0.1	0.5 ± 0.1	0.7 ± 0.1	11.4 ± 0.1
Pt/AC10PRR	87.6 ± 0.2	0.5 ± 0.1	0.5 ± 0.1	0.6 ± 0.1	10.8 ± 0.2
Pt/AC20PRR	88.0 ± 0.5	0.6 ± 0.1	0.6 ± 0.1	0.6 ± 0.1	10.2 ± 0.5
Pt/AC40PRR	86.1 ± 0.5	0.8 ± 0.2	0.5 ± 0.1	0.6 ± 0.1	12.0 ± 0.4

<sup>a</sup>Calculated by difference

STEM images and the Pt NPs size distributions of the monometallic catalysts are depicted in Figure 2. Pt/AC showed the largest mean NPs diameter ( $d_m = 4.6$  nm) and also higher agglomeration of NPs in some STEM images (Figure S2) but agglomerated were not considered for the calculation of mean diameters and in the histograms. The catalysts prepared with the modified supports had smaller mean NPs diameter (1.8 – 3.5 nm) and narrower size distribution, which may indicate that metal dispersion was favoured in these supports by deposition of char from PRR acting as anchoring sites for metal precursors. According to the STEM results, the lowest mean NPs diameter and narrowest distribution, i.e. better metal dispersion, was obtained by impregnation of AC with 10 wt. % of PRR.

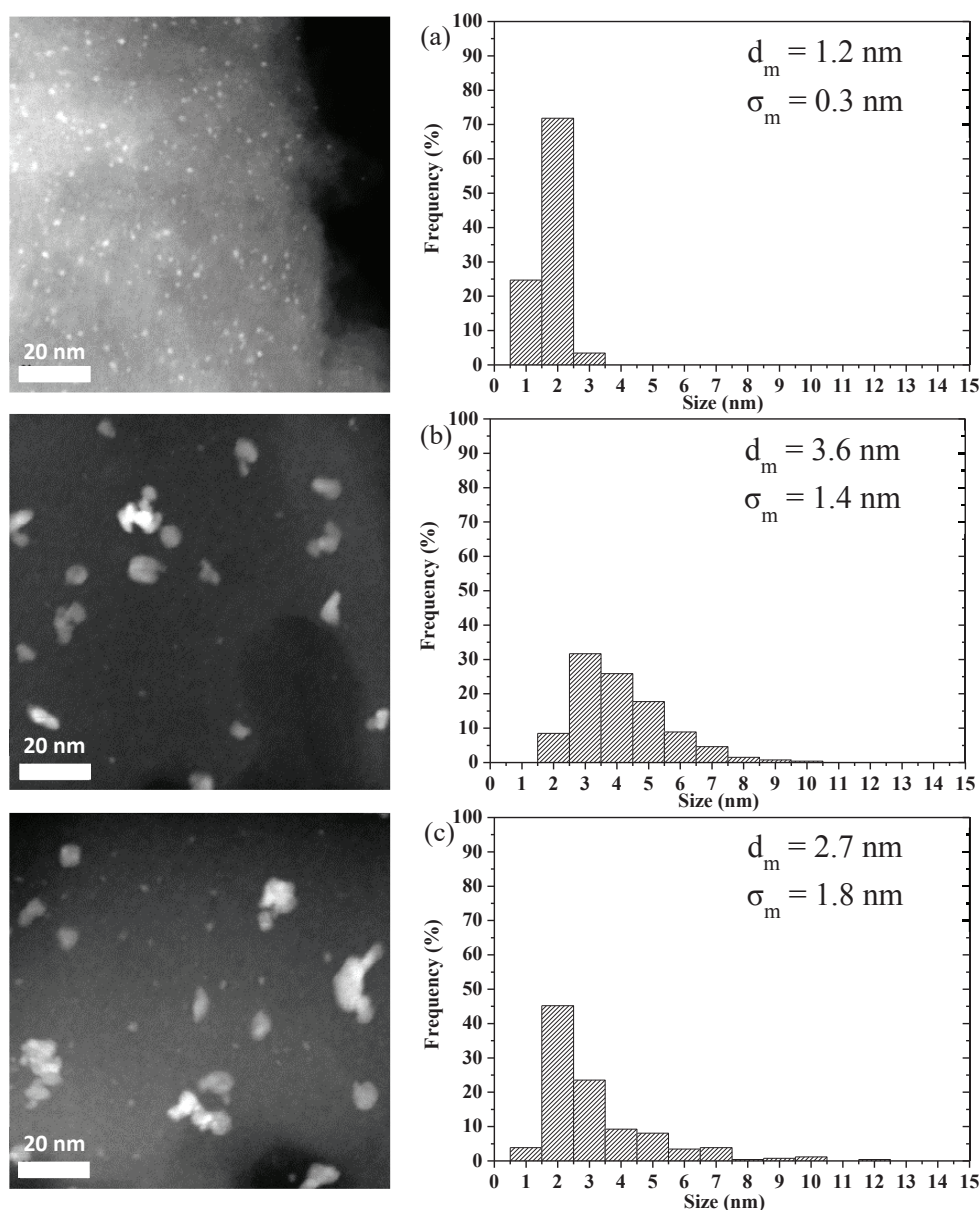


220

221 Figure 2. STEM images and NPs size distribution (a) Pt/AC, (b) Pt/AC1PRR, (c)  
 222 Pt/AC10PRR, (d) Pt/AC20PRR and (e) Pt/AC40PRR catalysts

223

224 Figure 3 displays the STEM images and NPs size distributions of the carbon-supported  
 225 PtRe catalysts. All bimetallic catalysts showed a smaller NPs size than Pt/AC, especially  
 226 1:1PtRe/AC (Figure 3 (a)), which exhibited a remarkably smaller mean NPs diameter ( $d_m$   
 227  $= 1.2$  nm) and the narrowest distribution ( $\sigma_m = 0.3$ ).



228

229 Figure 3. STEM images and NPs size distribution (a) 1:1PtRe/AC, (b) 1:2PtRe/AC and  
 230 (c) 2:1PtRe/AC catalysts

### 3.2. Catalytic performance vs porous texture

Different Pt catalysts prepared with modified supports (AC%PRR) were tested to learn about the role of the porous texture on the catalytic performance in APR. Figure 4 shows the progression of TOC removal upon TOS for these catalysts and for reference Pt/AC catalyst. Higher initial TOC removal values were obtained with Pt/AC%PRR catalysts, with maxima located at 1-2 h on stream, followed by monotonic decreases lasting several hours and final stabilization at values significantly lower than maxima. In contrast, for Pt/AC catalyst TOC removal gradually increased during the first 4 h on stream and then remained relatively constant at a higher value than Pt/AC%PRR catalysts, except in the case of Pt/AC10PRR. A clear trend related to the lower microporosity of the catalysts and TOC removal could not be deduced. Nevertheless, the addition of the PRR could have indirectly affected the catalyst performance since a direct correlation of the mean NPs diameter (Figure 2) and the maximum TOC removal (Figure 4) could be observed. Thus, the smaller the mean NPs diameter and higher the dispersion, the higher was the initial TOC removal achieved, and the following order of the maximum TOC removal was obtained: Pt/AC10PRR > Pt/AC1PRR > Pt/AC20PRR > Pt/AC40PRR > Pt/AC.

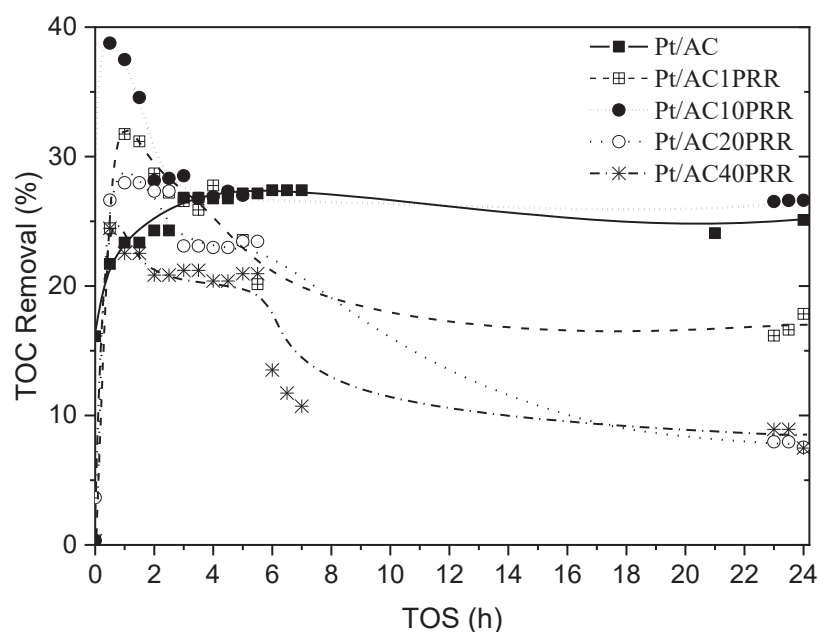


Figure 4. TOC removal upon time on stream in the APR of SBW with Pt/AC and Pt/AC%PRR catalysts

Regarding the gas products, Pt/AC%PRR catalysts showed higher CC gas values than Pt/AC, however the values were low in all experiments and significantly decreased after a short TOS (Figure 5), which is in accordance with TOC removal and evidence deactivation. The catalyst with AC support impregnated with 1 wt. % of PRR (Pt/AC1PRR) showed the highest CC gas (6.3 %) and this parameter decreased at increasing percentage of PRR, although the values were fairly similar for PRR percentages above 1 wt. %.

The carbon balance closure in the experiments described above matched from 64 to 100 %. Discrepancies between carbon removed from SBW and carbon detected in the gas products can be attributed to the formation of solid phase upon hydrothermal carbonization (HTC), adsorption of compounds and/or deposition of condensation and polymerization species, which contributes to catalysts deactivation. In this sense, some



relevant precursors of solid humins, such as glucose, pyruvaldehyde and hydroxymethylfurfural (HMF), were detected in the APR of maltose, the main compound of SBW, evidencing the feasibility of solids formation [45].

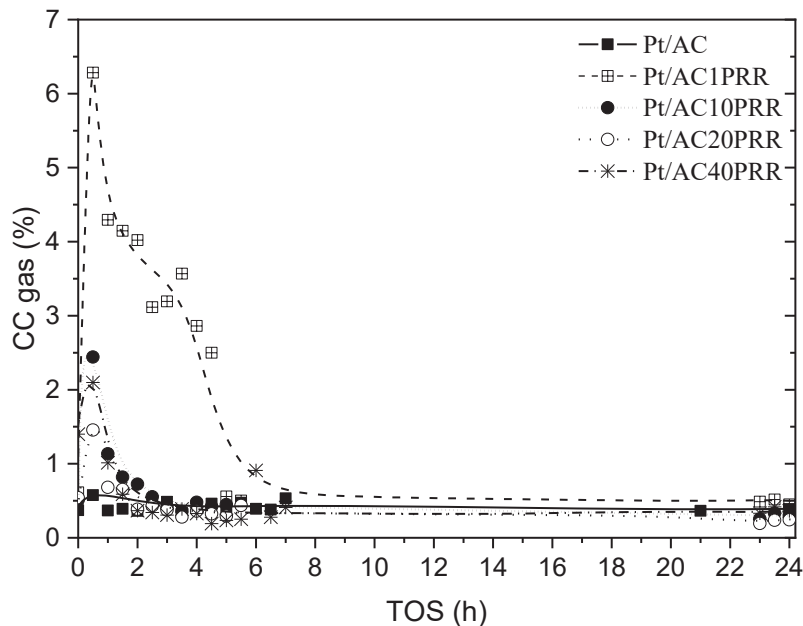


Figure 5. CC gas upon time on stream in the APR of SBW with Pt/AC and Pt/AC%PRR catalysts

Figure 6 shows the  $H_2$ , total alkanes and  $CO_2$  production upon TOS. Catalytic activity reached peak values at short TOS and then decayed sharply, as it was also observed for CC gas, suggesting a common deactivation mechanism. During the first hours on stream, Pt/AC%PRR catalysts achieved higher  $H_2$  production than Pt/AC, consistent with the fact that their less microporous texture could facilitate the transport of reactants to the active sites and gas products out of the catalyst. At short TOS values, Pt/AC40PRR catalyst yielded the highest  $H_2$  production ( $11.5 \mu\text{mol min}^{-1}$  corresponding to  $1.7 \text{ mmol } H_2 \text{ gCOD}_{\text{initial}}^{-1}$ ), whereas a significantly lower production ( $1.9 \mu\text{mol min}^{-1}$  corresponding to

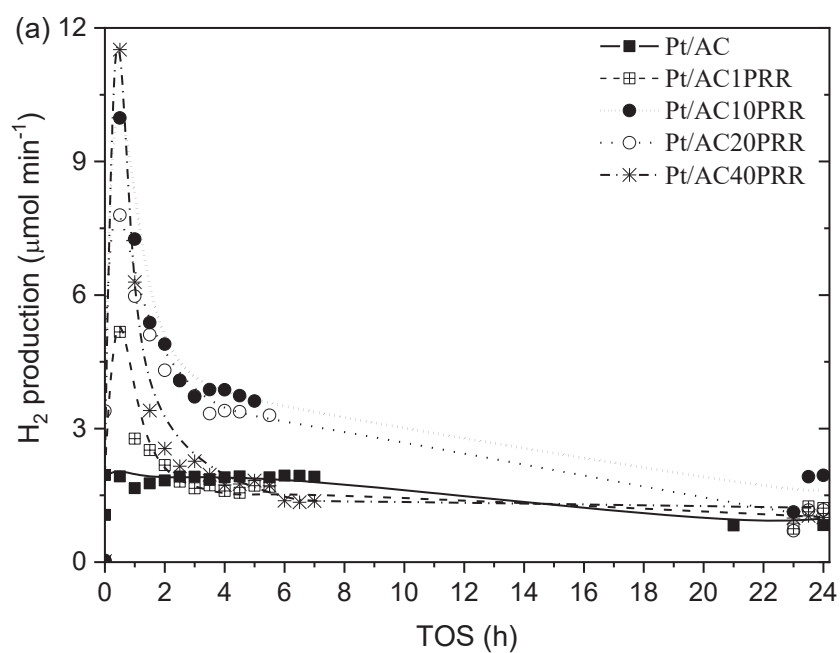


0.3 mmol H<sub>2</sub> gCOD<sub>initial</sub><sup>-1</sup>) was achieved with Pt/AC. Although the microporosity decreased at increasing the percentage of PRR added to the support, the order of maximum H<sub>2</sub> production at lower TOS values was Pt/AC40PRR > Pt/AC10PRR > Pt/AC20PRR > Pt/AC1PRR > Pt/AC. Therefore, Pt/AC10PRR showed a higher maximum H<sub>2</sub> production (10.0 μmol min<sup>-1</sup>) than Pt/AC20PRR (7.8 μmol min<sup>-1</sup>), despite having a higher microporosity. This result could be related to the crossed effect of Pt NPs in these catalysts, clearly smaller for Pt/AC10PRR. Kim *et al.* [46] reported higher catalytic activity and stability in the APR of xylose using a Pt catalyst with an average particle size of 1.3 nm compared to one of 4 nm. Chen *et al.* [47] also reported higher catalytic activity and H<sub>2</sub> selectivity in the APR of the low-boiling fraction of bio-oil when the mean Pt NPs size decreased from 5.7 nm to 1.6 nm. They proposed that in small Pt NPs the edge sites can provide with more stable Pt-C bonds that facilitate C-C bond cleavage, leading to higher H<sub>2</sub> formation. On the contrary, Ciftci *et al.* [48] analysed the effect of Pt NPs size in the APR of glycerol by varying NP size from 1.2 to 4.2 nm and found that the catalyst with an intermediate NP size of 2 nm exhibited optimum activity for H<sub>2</sub> production due to optimum C-C bond cleavage rates. Therefore, the highest maximum H<sub>2</sub> production of Pt/AC10PRR catalyst, respect to the Pt/AC20PRR, could be ascribed to its mean Pt NPs size closer to this reported optimum of 2 nm.

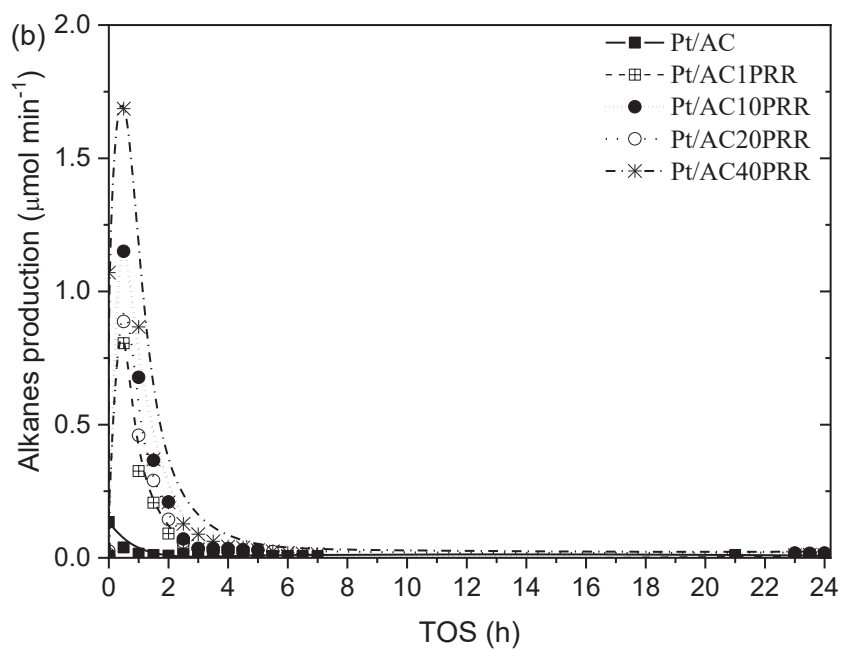
Regarding alkanes production, at short TOS values the catalysts exhibited a similar trend to that of H<sub>2</sub> production. However, production decreased sharply to almost negligible values in all the experiments, indicating that deactivation affected alkane production more than H<sub>2</sub> production. Pt/AC40PRR catalyst achieved a maximum of alkanes production of around 1.7 μmol min<sup>-1</sup> (87 mol % CH<sub>4</sub>) at around 1 h on stream, in contrast to that of Pt/AC, which showed a significantly lower production (0.04 μmol min<sup>-1</sup>). Concerning CO<sub>2</sub> production, it was much larger for Pt/AC1PRR and a main contribution to the high

304 CC gas observed for this catalyst. It must be recalled that CO<sub>2</sub> evolution is slightly  
 305 underestimated as it is affected by KOH added to SBW [41].

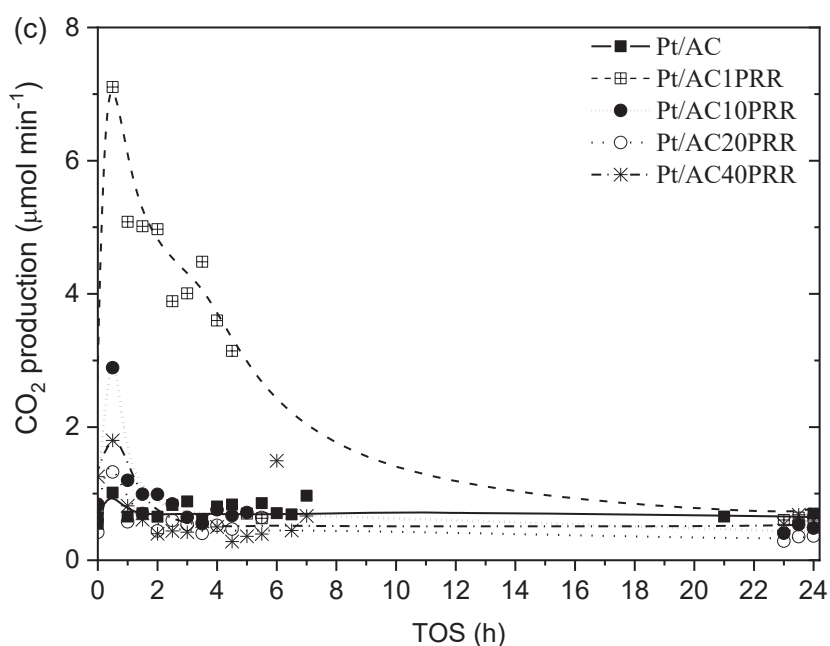
306



307



308



309

310 Figure 6. (a) H<sub>2</sub>, (b) total alkanes production and (c) CO<sub>2</sub> upon time on stream in the APR  
 311 of SBW with Pt/AC and Pt/AC%PRR catalysts

312

### 313 3.3. Catalytic performance vs type of active phase

314 Figure 7 shows TOC removal upon TOS with Pt/AC catalyst and PtRe/AC catalysts with  
 315 different Pt and Re loads, under the same conditions of the previous experiments. The  
 316 highest TOC removal was achieved with 1:1PtRe/AC catalyst at short TOS values, but a  
 317 pronounced decay of its performance was observed after only 2 h on stream. Catalyst 1:2  
 318 PtRe/AC showed a similar behaviour but achieved lower TOC removal within the whole  
 319 TOS range. On the contrary, the catalyst with the lowest load of Re (2:1PtRe/AC), showed  
 320 a similar trend to that observed with Pt/AC. Both catalysts showed a gradual increase in  
 321 TOC removal values in the short TOS range, and then a plateau evidencing low  
 322 deactivation. Thus, the Re addition seems to favour catalysts deactivation, , probably  
 323 because the acid sites of the PtRe/AC catalysts can promote the formation of coke  
 324 precursors, as it was reported in previous studies [49,50]. In this sense, a possible pathway

for coke formation could be due to an increase in dehydration reactions favoured by the surface acidity of PtRe alloy [13,51]. Dehydration of sugars, like glucose, xylose and fructose, leads to formation of furfural and HMF, which can form molecules with long unsaturated bonds by the aldol condensation reaction [14]. These larger molecules can easily grow-up towards condensed structures giving rise to coke formation [15], leading to catalyst deactivation.

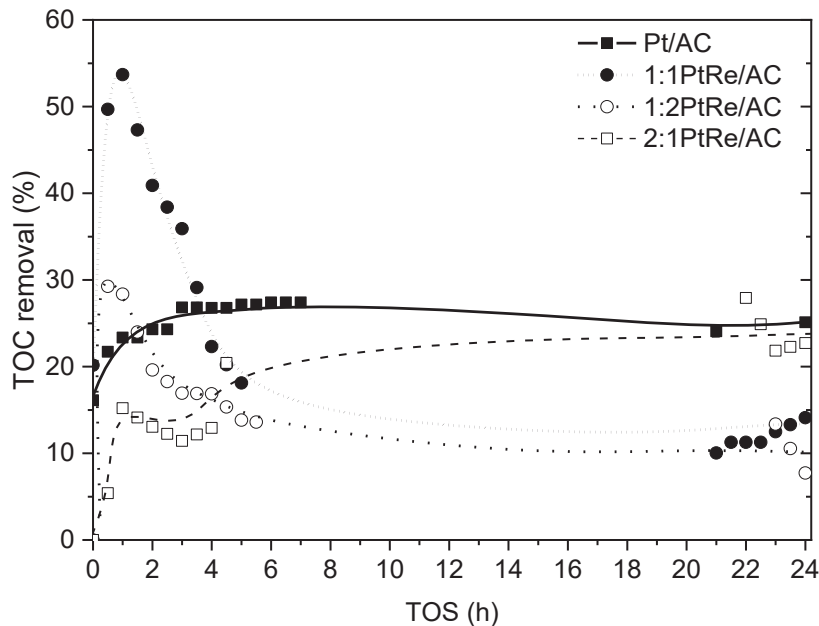


Figure 7. TOC removal upon time on stream in the APR of SBW with Pt and PtRe catalysts

The evolution of CC gas upon TOS is shown in Figure 8. All the PtRe catalysts yielded much higher CC gas values than Pt one, but the gas production occurred only within a narrow TOS range. After 4 h TOS only 1:1PtRe/AC maintained significant production, although in a low amount (ca. 1 %). The carbon balance closure in these experiments ranged from 73 to 100 %. As observed in the previous experiments, the lack of carbon balance closure can be attributed to the formation of solid deposits.

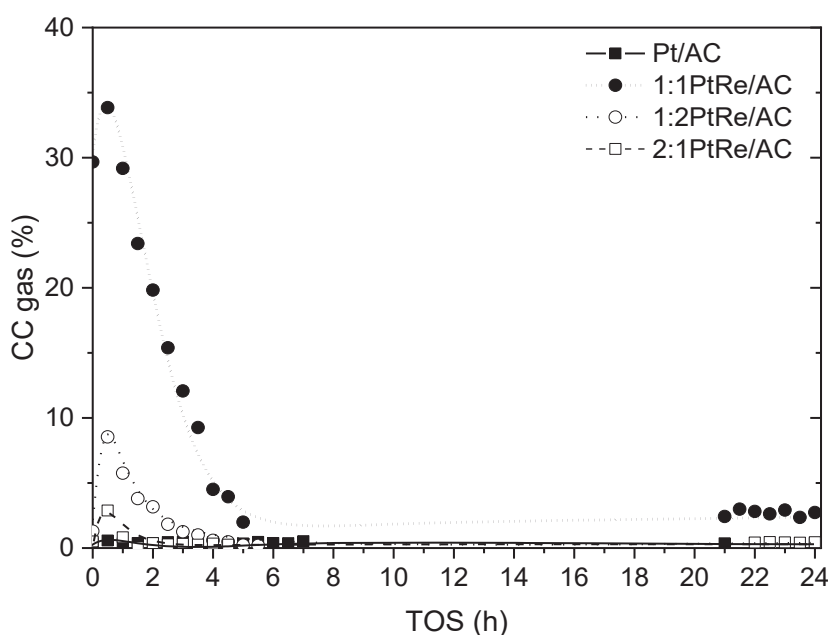
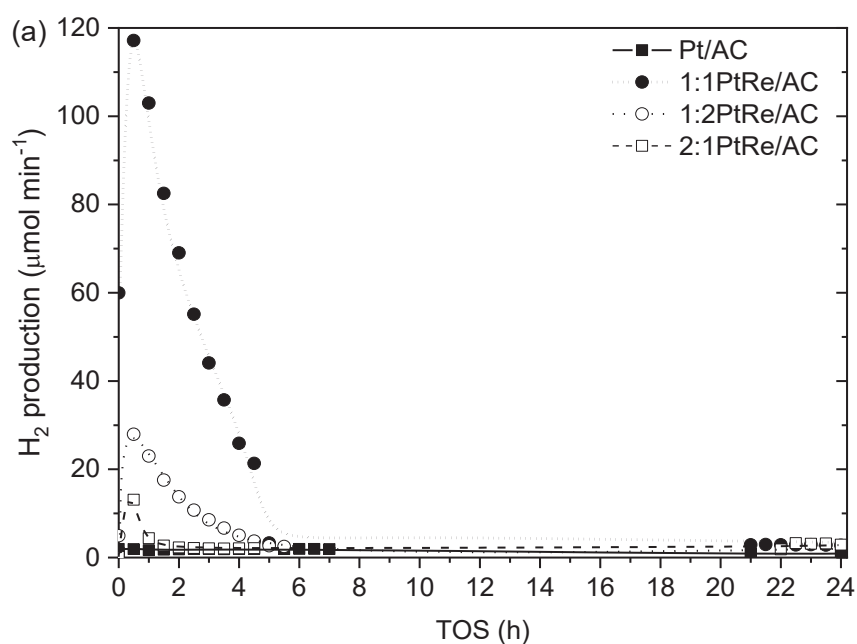


Figure 8. CC gas upon time on stream in the APR of SBW with Pt and PtRe catalysts

The production of  $H_2$ , total alkanes and  $CO_2$  upon TOS is shown in Figure 9. As expected, the trend is consistent with the evolution of CC gas and confirms deactivation of the catalysts. The small residual production of gases, consisting mainly of  $CO_2$ , can be attributed almost completely to HTC, since this process gives rise mostly to char and low gas production, essentially  $CO_2$ . HTC is also responsible for TOC removal at long TOS values.

Several authors [13,44,51] have reported an increase in APR catalytic performance for PtRe/C catalysts compared to Pt/C ones. This catalytic performance boost was attributed to enhanced WGS reaction due to Re addition to Pt catalyst, mainly due to higher activity in water activation, which is an important step of WGS reaction. This could explain the higher short-term  $H_2$  production with PtRe/AC catalysts in Figure 9. On the other hand, other authors [44,51] have observed a decrease in  $H_2$  selectivity due to higher dehydration reactions rates facilitated by the surface acidity promoted by Re addition. In the current

work, 1:1PtRe/AC achieved the highest gas production values among the catalysts tested, with a maximum of  $117.2 \mu\text{mol min}^{-1}$  for  $\text{H}_2$  (corresponding to  $17.9 \text{ mmol H}_2 \text{ gCOD}_{\text{initial}}^{-1}$ ) and  $24.5 \mu\text{mol min}^{-1}$  (96 mol %  $\text{CH}_4$ ) for alkanes, both around the first hour on stream. Finally, the quite similar patterns observed with all the catalysts regarding to the gas products production suggest similar ways of deactivation despite the differences in the metal active phase.



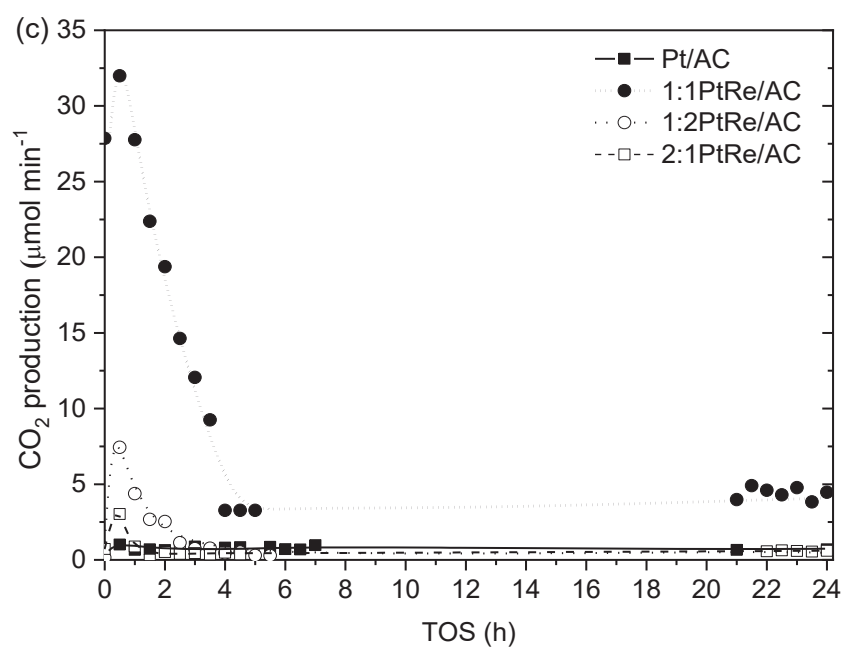
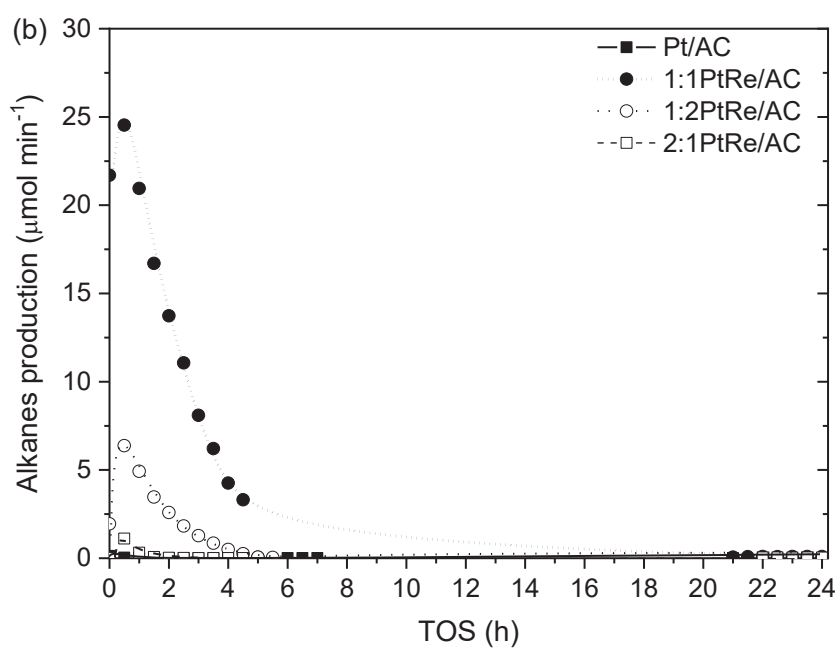


Figure 9. (a)  $\text{H}_2$ , (b) total alkanes and (c)  $\text{CO}_2$  production upon time on stream in the APR of SBW with Pt and PtRe catalysts

369 Finally, it is important to mention that the addition of Re to Pt catalysts can significantly  
370 change the products distribution. Ciftci *et al.* [13] and Zhang *et al.* [43] reported that in  
371 the APR of glycerol this addition of Re mainly increased the selectivity toward  $C_2^+$   
372 alkanes (ethane and propane), carboxylic acids and alcohols at the expense of selectivity  
373 to  $H_2$ ,  $CH_4$  and  $CO_2$ . In the current work, the alkanes distribution of the Pt and Pt Re  
374 catalysts was also different. In all the experiments,  $CH_4$  was the major compound in the  
375 alkanes fraction (Figure 10). At short TOS (up to 5 h), when the catalysts still had  
376 significant activity,  $CH_4$  percentage ranged between 68 and 98 mol %, being substantially  
377 higher with PtRe catalysts (between 92 – 98 mol %) than with Pt catalyst. The addition  
378 of KOH to SBW could have affected the production of  $C_2^+$  alkanes, since some authors  
379 have reported that the presence of bases in the reaction medium disfavours the formation  
380 pathway of these compounds, probably affecting dehydration followed by hydrogenation  
381 of alcohols [44]. This effect could be more significant in the case of bimetallic catalysts,  
382 since the addition of KOH could neutralize the surface acidity associated to the PtRe  
383 alloy, thus partially suppressing the dehydration pathways [43,44].



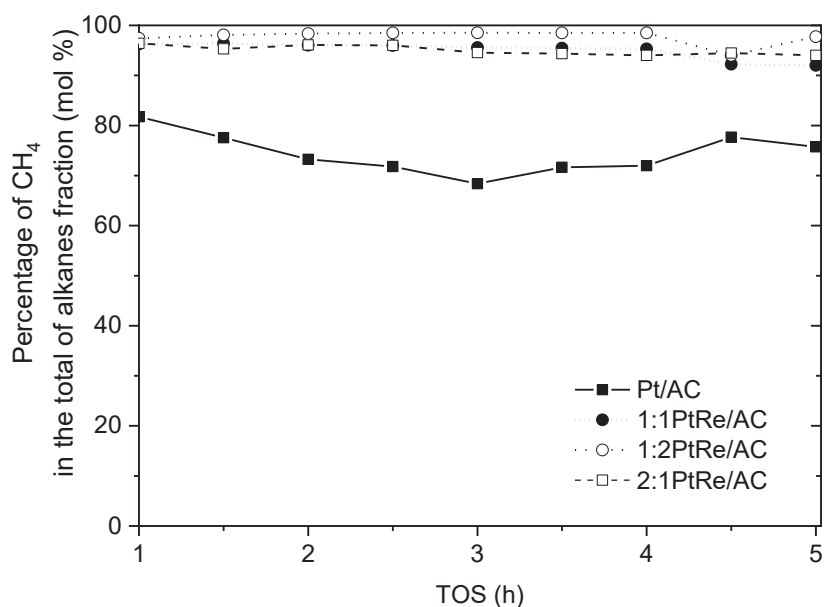


Figure 10.

Percentage of CH<sub>4</sub> in the total of alkanes fraction upon time on stream in the APR of SBW with Pt and PtRe catalysts

### 3.4. Deactivation of catalysts

Despite the different metal active phases and supports tested, catalyst deactivation was observed with TOS. Therefore, to evaluate the potential factors that affect the stability of the catalysts, they were characterized after use. The N<sub>2</sub> adsorption/desorption isotherms showed a dramatic loss of surface area for all catalysts after 24 h on stream. As a representative example, Table 3 shows the textural characteristics of fresh and used 1:1PtRe/AC catalyst. After 1 h on stream, this catalyst lost around 25 % of the initial S<sub>BET</sub> and after 24 h APR the remaining surface area was only 3.5 % of the initial value, with complete loss of the microporosity. A similar situation was observed for the rest of the catalysts tested, most probably due to adsorption of compounds and/or formation of carbonaceous deposits on the catalysts surface, as previously proposed. This must be one of the main causes of the relevant and early deactivation observed in the APR experiments

using complex feedstocks, as suggested in previous studies on APR of brewery wastewater [32] and sugar-based biorefinery streams [52] using Pt/C catalysts. This assumption is also supported by previous works where under similar APR conditions metal active leaching was negligible [32] and only small changes in the electrodeposited to zerovalent Pt ratio (obtained by XPS characterization) were observed after successive APR cycles [32,53].

Table 3. Pore texture of fresh and used 1:1PtRe/AC catalyst

Samples	$S_{BET}$ ( $m^2 g^{-1}$ )	$A_{EXT}$ ( $m^2 g^{-1}$ )	Micropore volume ( $cm^3 g^{-1}$ )	Mesopore volume ( $cm^3 g^{-1}$ )
1:1PtRe/AC fresh	820	120	0.34	0.15
1:1PtRe/AC 1 h on stream	610	100	0.26	0.12
1:1PtRe/AC 24 h on stream	30	30	<0.001	0.05

The stability of the metal active phase was assessed from STEM characterization. Table 4 shows the mean NPs size of the fresh and used catalysts (after 24 h on stream), while the STEM images and the corresponding histograms representing NPs size distribution are included as Supplementary Material (Figure S3). The mean Pt NPs size of Pt/AC catalyst moderately increased ( $\approx 22\%$ ) after 24 h on stream, suggesting some metal sintering. Pt/AC%PRR catalysts showed larger mean NPs size after use, except in the case of Pt/AC40PRR catalyst, for which no significant changes were observed. However, it is worth highlighting that some agglomeration of NPs was observed in some catalysts, although it was not considered to build the histograms in Figure S3. In the case of 1:1PtRe/AC catalyst, only a slight increase of mean NPs size was observed after 1 h on stream, without significant change throughout the whole 24 h TOS range tested. After 24 h on stream 1:2PtRe/AC catalyst yielded smaller mean NPs size than the fresh one. As previously reported in literature [54], the smaller NP size of the PtRe catalysts indicate a

stabilization of Pt against sintering by the presence of Re. Based on the results presented, it is unlikely that the very low to moderate changes in the mean NPs size of catalysts during use are responsible for the deactivation observed.

Table 4. Mean NPs size of the fresh and used catalysts

Samples	Mean NPs size (nm)	
	Fresh	Used (24 h on stream)
Pt/AC	$4.6 \pm 2.2$	$5.6 \pm 5.2$
Pt/AC10PRR	$1.8 \pm 0.7$	$4.3 \pm 1.8$
Pt/AC20PRR	$3.1 \pm 1.5$	$4.1 \pm 3.3$
Pt/AC40PRR	$3.5 \pm 1.6$	$3.3 \pm 2.0$
1:1PtRe/AC	$1.2 \pm 0.3$	$1.5 \pm 0.4^a$
1:2PtRe/AC	$3.6 \pm 1.4$	$1.7 \pm 0.6$

<sup>a</sup>1 h on stream

Figure 11 shows the TG-TPD profiles and the corresponding differential curves (DTG) for the fresh and used Pt/AC, Pt/AC40PRR and 1:1PtRe/AC catalysts. The TG-TPO profiles, with the corresponding differential curves, are depicted in Figure 12. The quantitative weight loss values are summarized in the Supplementary Material (Table S1).

The initial peak in the TG/DTG-TPD profiles can be attributed to loss of water adsorbed on the catalysts (Figure 11). Beyond 100 °C, the fresh catalysts did not show relevant weight loss, which indicates a good thermal stability. On the contrary, the used catalysts showed a significant peak ranging from about 150 to 425 °C, which can be ascribed to the loss of reactants and/or products physically adsorbed on the catalyst surface or coke precursor species.

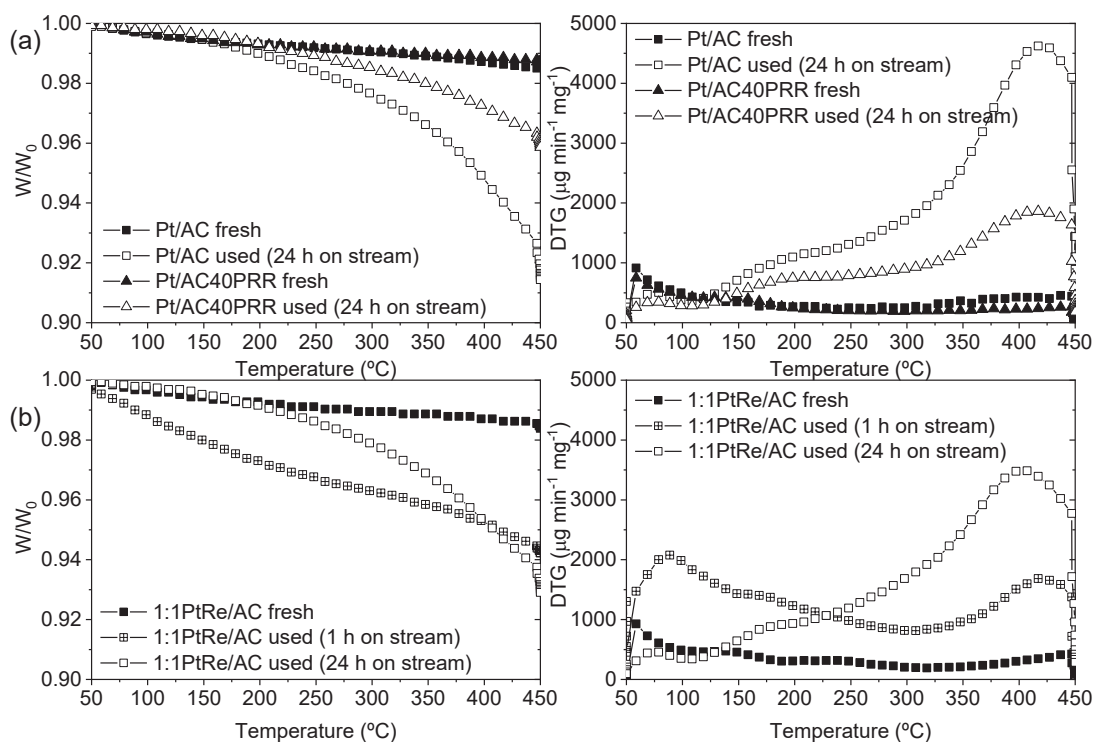
In the DTG-TPD profiles, the main peak was located around 425 °C for both Pt/AC and Pt/AC40PRR used catalyst. However, the high relative intensity of the peak at around

150 °C observed for Pt/AC40PRR indicates a lower degree of structure development of the deposits or species uptaken on this catalyst (Figure 11 (a)). The percentages of weight loss in the TG-TPD profiles increased from 1.4 and 1.9 % to 4.1 and 8.6 % for the fresh and used Pt/AC40PRR and Pt/AC catalysts, respectively (Table S1). These results indicate that the lower porosity of the AC40PRR support, due to PRR infiltration and carbonization, decreased the amount of adsorbed species and prevented their development, but this was not enough to avoid deactivation.

In the TG-TPO profile of Pt/AC40PRR (Figure 12 (a)), an earlier and sharper decrease in the sample weight was observed than for Pt/AC. The pattern is similar for the fresh and used Pt/AC40PRR, showing that part of the oxidation at lower temperature is associated to the carbon deposited by carbonisation of infiltrated PRR. However, the shift of the main peak to lower combustion temperatures for used catalyst also suggests light species deposited on its surface.

Regarding DTG-TPD/TPO profiles of 1:1PtRe/AC catalyst after 1 and 24 h on stream (Figure 11 (b) and Figure 12 (b)), a clear aging effect of the deposited species could be observed as TOS increased. An increase in the evolution of species by TPD was observed, with a maximum located at 400 °C, and the shift of the main peak to higher combustion temperatures in the TPD corroborates this aging effect. The percentages of weight loss in the TG-TPD profiles increased from 1.6 %, for the fresh catalyst, to 5.8 and 7.1 % for the used catalysts at 1 h and 24 h on stream, respectively (Table S1). Re addition also appears to accelerate the combustion of the support, yielding a similar sharp peak in the DTG-TPO profile (Figure 12 (b)). Therefore, the adsorption of species and/or the formation of coke-like deposits on the catalyst surface must be a main cause of the strong and early deactivation observed in the APR experiments under the reaction conditions tested. Thus, the perspectives of future studies of APR of biowaste streams should be related to the

466 evaluation of reaction conditions or combined processes that can avoid deactivation or  
 467 allow regeneration of the catalysts.



468

469 Figure 11. TG-TPD profiles and corresponding derivative curves of the fresh and used  
 470 (a) Pt/AC and Pt/AC40PRR catalyst and (b) 1:1PtRe/AC catalysts

471

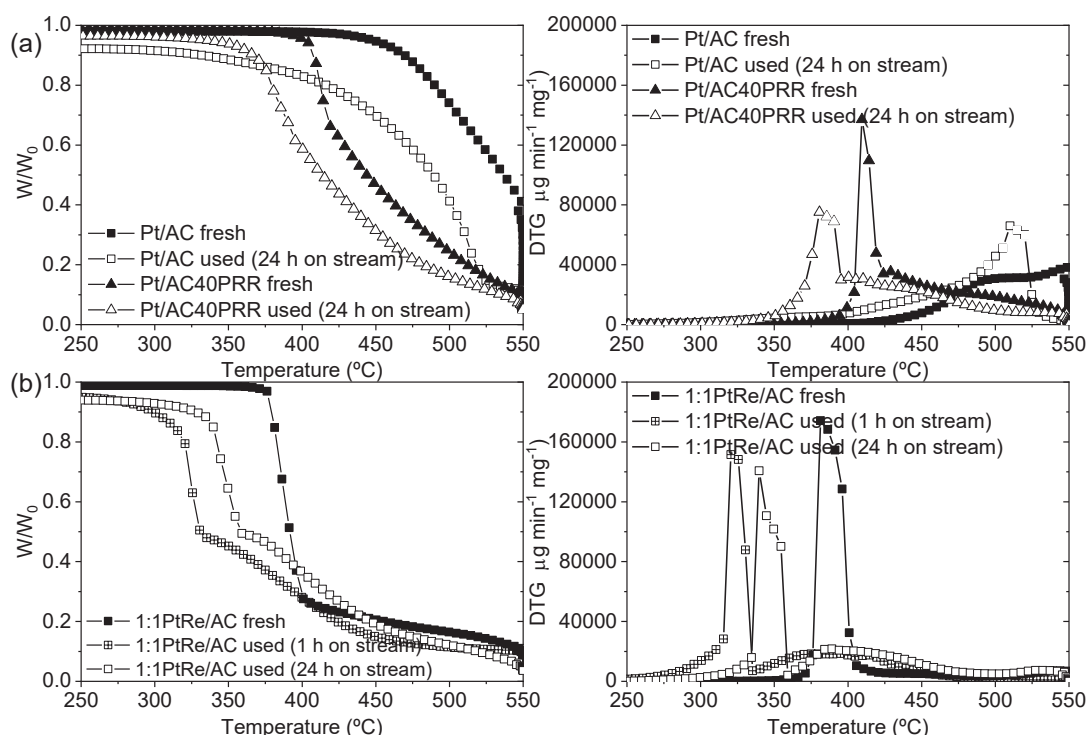


Figure 12. TG-TPO profiles and corresponding derivative curves of fresh and used (a) Pt/AC and Pt/AC40PRR catalyst and (b) 1:1PtRe/AC catalysts

## 4. Conclusions

The stability and the performance of carbon-supported Pt and PtRe catalysts in the APR of wastewater streams was evaluated using brewery wastewater as a feedstock. Despite the different textural properties of the supports and the different metal active phase tested, a significant catalysts deactivation was observed with TOS.

At low TOS values, the catalysts synthesised with the modified supports (Pt/AC%PRR) showed higher  $H_2$  production than the catalyst synthesized with the AC support, indicating that a lower microporosity facilitated the transport of reactants and products,

increasing gas production. Furthermore, a crossed effect of Pt NP size on H<sub>2</sub> production was observed.

All PtRe catalysts showed a higher activity than Pt/AC. Catalyst 1:1PtRe/AC showed the highest gas production, with a maximum of H<sub>2</sub> production of 117.2 μmol min<sup>-1</sup> ≈ 17.9 mmol H<sub>2</sub> gCOD<sub>initial</sub><sup>-1</sup>. Nevertheless, the Re addition to Pt/AC catalyst seems to favour catalyst deactivation, probably due to the formation of organic molecules with long unsaturated bonds that can evolve towards coke formation.

The characterization of used catalysts allowed identifying adsorption of organic species and/or coke-like matter deposition on the catalysts surface as the main cause of deactivation. An important loss of S<sub>BET</sub> was observed in the first hour on stream and a clear aging effect of the deposited species was observed with TOS, while the leaching, sintering or oxidation of active phase are unlikely to be responsible for the observed deactivation.

## Acknowledgements

The authors greatly appreciate financial support from Spanish MINECO (CTQ2015-65491-R) and Comunidad de Madrid (BIOTRES-CM P2018/EMT-4344). A. S. Oliveira thanks the Spanish MINECO a research grant (BES-2016-077244).

## References

- [1] Momirlan M, Veziroglu TN. The properties of hydrogen as fuel tomorrow in sustainable energy system for a cleaner planet. Int J Hydrogen Energy

507 2005;30:795–802. <https://doi.org/10.1016/J.IJHYDENE.2004.10.011>.

508 [2] Marchenko OV, Solomin SV. The future energy: Hydrogen versus electricity. *Int*  
509 *J Hydrogen Energy* 2015;40:3801–5.  
510 <https://doi.org/10.1016/J.IJHYDENE.2015.01.132>.

511 [3] Balat H, Kirtay E. Hydrogen from biomass – Present scenario and future prospects.  
512 *Int J Hydrogen Energy* 2010;35:7416–26.  
513 <https://doi.org/10.1016/J.IJHYDENE.2010.04.137>.

514 [4] Nicoletti G, Arcuri N, Nicoletti G, Bruno R. A technical and environmental  
515 comparison between hydrogen and some fossil fuels. *Energy Convers Manag*  
516 2015;89:205–13. <https://doi.org/10.1016/J.ENCONMAN.2014.09.057>.

517 [5] Cortright RD, Davda RR, Dumesic JA. Hydrogen from catalytic reforming of  
518 biomass-derived hydrocarbons in liquid water. *Nature* 2002;418:964–7.  
519 <https://doi.org/10.1038/nature01009>.

520 [6] Khodabandehloo M, Larimi A, Khorasheh F. Comparative process modeling and  
521 techno-economic evaluation of renewable hydrogen production by glycerol  
522 reforming in aqueous and gaseous phases. *Energy Convers Manag*  
523 2020;225:113483. <https://doi.org/10.1016/j.enconman.2020.113483>.

524 [7] Davda RR, Shabaker JW, Huber GW, Cortright RD, Dumesic JA. A review of  
525 catalytic issues and process conditions for renewable hydrogen and alkanes by  
526 aqueous-phase reforming of oxygenated hydrocarbons over supported metal  
527 catalysts. *Appl Catal B Environ* 2005;56:171–86.  
528 <https://doi.org/10.1016/j.apcatb.2004.04.027>.

529 [8] Davda RR, Shabaker JW, Huber GW, Cortright RD, Dumesic JA. Aqueous-phase  
530 reforming of ethylene glycol on silica-supported metal catalysts. *Appl Catal B*  
531 *Environ* 2003;43:13–26. [https://doi.org/10.1016/S0926-3373\(02\)00277-1](https://doi.org/10.1016/S0926-3373(02)00277-1).



- 532 [9] Xu C, Paone E, Rodríguez-Padrón D, Luque R, Mauriello F. Reductive catalytic  
533 routes towards sustainable production of hydrogen, fuels and chemicals from  
534 biomass derived polyols. *Renew Sustain Energy Rev* 2020;127:109852.  
535 <https://doi.org/10.1016/j.rser.2020.109852>.
- 536 [10] Huber GW, Shabaker JW, Evans ST, Dumesic JA. Aqueous-phase reforming of  
537 ethylene glycol over supported Pt and Pd bimetallic catalysts. *Appl Catal B*  
538 *Environ* 2006;62:226–35. <https://doi.org/10.1016/j.apcatb.2005.07.010>.
- 539 [11] Godina LI, Kirilin A V., Tokarev A V., Simakova IL, Murzin DY. Sibunit-  
540 supported mono- and bimetallic catalysts used in aqueous-phase reforming of  
541 xylitol. *Ind Eng Chem Res* 2018;57:2050–67.  
542 <https://doi.org/10.1021/acs.iecr.7b04937>.
- 543 [12] Kaya B, Irmak S, Hasanoglu A, Erbatur O. Developing Pt based bimetallic and  
544 trimetallic carbon supported catalysts for aqueous-phase reforming of biomass-  
545 derived compounds. *Int J Hydrogen Energy* 2015;40:3849–58.  
546 <https://doi.org/10.1016/j.ijhydene.2015.01.131>.
- 547 [13] Ciftci A, Ligthart DAJM, Hensen EJM. Aqueous phase reforming of glycerol over  
548 Re-promoted Pt and Rh catalysts. *Green Chem* 2014;16:853–63.  
549 <https://doi.org/10.1039/C3GC42046A>.
- 550 [14] Chheda JN, Dumesic JA. An overview of dehydration, aldol-condensation and  
551 hydrogenation processes for production of liquid alkanes from biomass-derived  
552 carbohydrates. *Catal Today* 2007;123:59–70.  
553 <https://doi.org/10.1016/j.cattod.2006.12.006>.
- 554 [15] Koichumanova K, Vikla AKK, Cortese R, Ferrante F, Seshan K, Duca D, et al. In  
555 situ ATR-IR studies in aqueous phase reforming of hydroxyacetone on Pt/ZrO<sub>2</sub>  
556 and Pt/AlO(OH) catalysts: The role of aldol condensation. *Appl Catal B Environ*

2018;232:454–63. <https://doi.org/10.1016/J.APCATB.2018.03.090>.

[16] Luo N, Fu X, Cao F, Xiao T, Edwards PP. Glycerol aqueous phase reforming for hydrogen generation over Pt catalyst – Effect of catalyst composition and reaction conditions. *Fuel* 2008;87:3483–9. <https://doi.org/10.1016/j.fuel.2008.06.021>.

[17] Kirilin A V., Tokarev A V., Murzina E V., Kustov LM, Mikkola JP, Murzin DY. Reaction products and transformations of intermediates in the aqueous-phase reforming of sorbitol. *ChemSusChem* 2010;3:708–18. <https://doi.org/10.1002/cssc.200900254>.

[18] Shabaker JW, Davda RR, Huber GW, Cortright RD, Dumesic JA. Aqueous-phase reforming of methanol and ethylene glycol over alumina-supported platinum catalysts. *J Catal* 2003;215:344–52. [https://doi.org/10.1016/S0021-9517\(03\)00032-0](https://doi.org/10.1016/S0021-9517(03)00032-0).

[19] Shabaker JW, Dumesic JA. Kinetics of Aqueous-Phase Reforming of Oxygenated Hydrocarbons: Pt/Al<sub>2</sub>O<sub>3</sub> and Sn-Modified Ni Catalysts. *Ind Eng Chem Res* 2004;43:3105–12. <https://doi.org/10.1021/ie049852o>.

[20] Duarte HA, Sad ME, Apesteguía CR. Bio-hydrogen production by APR of C<sub>2</sub>-C<sub>6</sub> polyols on Pt/Al<sub>2</sub>O<sub>3</sub>: Dependence of H<sub>2</sub> productivity on metal content. *Catal Today* 2017;296:59–65. <https://doi.org/10.1016/j.cattod.2017.04.067>.

[21] Aho A, Rosales C, Eränen K, Salmi T, Murzin DY, Grénman H. Biohydrogen from dilute side streams - Influence of reaction conditions on the conversion and selectivity in aqueous phase reforming of xylitol. *Biomass and Bioenergy* 2020;138:105590. <https://doi.org/10.1016/j.biombioe.2020.105590>.

[22] M. Ravenelle R, R. Copeland J, Kim W-GG, C. Crittenden J, Sievers C, Ravenelle RM, et al. Structural changes of  $\gamma$ -Al<sub>2</sub>O<sub>3</sub>-supported catalysts in hot liquid water. *ACS Catal* 2011;1:552–61. <https://doi.org/10.1021/cs1001515>.

- 582 [23] Ciftci A, Peng B, Jentys A, Lercher JA, Hensen EJM. Support effects in the  
583 aqueous phase reforming of glycerol over supported platinum catalysts. *Appl Catal*  
584 *A Gen* 2012;431–432:113–9. <https://doi.org/10.1016/j.apcata.2012.04.026>.
- 585 [24] El Doukkali M, Iriondo A, Cambra JF, Gandarias I, Jalowiecki-Duhamel L,  
586 Dumeignil F, et al. Deactivation study of the Pt and/or Ni-based  $\gamma$ -Al<sub>2</sub>O<sub>3</sub> catalysts  
587 used in the aqueous phase reforming of glycerol for H<sub>2</sub> production. *Appl Catal A*  
588 *Gen* 2014;472:80–91. <https://doi.org/10.1016/j.apcata.2013.12.015>.
- 589 [25] Liu F, Okolie C, Ravenelle RM, Crittenden JC, Sievers C, Bruijninx PCA, et al.  
590 Silica deposition as an approach for improving the hydrothermal stability of an  
591 alumina support during glycerol aqueous phase reforming. *Appl Catal A Gen*  
592 2018;551:13–22. <https://doi.org/10.1016/J.APCATA.2017.11.025>.
- 593 [26] Kim MC, Kim TW, Kim HJ, Kim CU, Bae JW. Aqueous phase reforming of  
594 polyols for hydrogen production using supported Pt-Fe bimetallic catalysts. *Renew*  
595 *Energy* 2016;95:396–403. <https://doi.org/10.1016/j.renene.2016.04.020>.
- 596 [27] Meryemoglu B, Irmak S, Hasanoglu A. Production of activated carbon materials  
597 from kenaf biomass to be used as catalyst support in aqueous-phase reforming  
598 process. *Fuel Process Technol* 2016;151:59–63.  
599 <https://doi.org/10.1016/j.fuproc.2016.05.040>.
- 600 [28] Jeong KE, Kim HD, Kim TW, Kim JW, Chae HJ, Jeong SY, et al. Hydrogen  
601 production by aqueous phase reforming of polyols over nano- and micro-sized  
602 mesoporous carbon supported platinum catalysts. *Catal Today* 2014;232:151–7.  
603 <https://doi.org/10.1016/j.cattod.2014.02.005>.
- 604 [29] Kim T-W, Kim H-D, Jeong K-E, Chae H-J, Jeong S-Y, Lee C-H, et al. Catalytic  
605 production of hydrogen through aqueous-phase reforming over platinum/ordered  
606 mesoporous carbon catalysts. *Green Chem* 2011;13:1718–28.

<https://doi.org/10.1039/c1gc15235a>.

- [30] Van Haasterecht T, Ludding CCI, De Jong KP, Bitter JH. Toward stable nickel catalysts for aqueous phase reforming of biomass-derived feedstock under reducing and alkaline conditions. *J Catal* 2014;319:27–35. <https://doi.org/10.1016/j.jcat.2014.07.014>.
- [31] Wang X, Li N, Zhang Z, Wang C, Pfefferle LD, Haller GL. High-yield hydrogen production from aqueous phase reforming over single-walled carbon nanotube supported catalysts. *ACS Catal* 2012;2:1480–6. <https://doi.org/10.1021/cs300274m>.
- [32] Oliveira ASS, Baeza JAA, Calvo L, Alonso-Morales N, Heras F, Rodriguez JJJ, et al. Production of hydrogen from brewery wastewater by aqueous phase reforming with Pt/C catalysts. *Appl Catal B Environ* 2019;245:367–75. <https://doi.org/10.1016/j.apcatb.2018.12.061>.
- [33] Van Haasterecht T, Ludding CCI, De Jong KP, Bitter JH. Stability and activity of carbon nanofiber-supported catalysts in the aqueous phase reforming of ethylene glycol. *J Energy Chem* 2013;22:257–69. [https://doi.org/10.1016/S2095-4956\(13\)60032-7](https://doi.org/10.1016/S2095-4956(13)60032-7).
- [34] Reynoso AJ, Ayastuy JL, Iriarte-Velasco U, Gutiérrez-Ortiz MA. Cobalt aluminate spinel-derived catalysts for glycerol aqueous phase reforming. *Appl Catal B Environ* 2018;239:86–101. <https://doi.org/10.1016/J.APCATB.2018.08.001>.
- [35] Stekrova M, Rinta-Paavola A, Karinen R. Hydrogen production via aqueous-phase reforming of methanol over nickel modified Ce, Zr and La oxide supports. *Catal Today* 2018;304:143–52. <https://doi.org/10.1016/J.CATTOD.2017.08.030>.
- [36] Shabaker JW, Huber GW, Dumesic J. Aqueous-phase reforming of oxygenated hydrocarbons over Sn-modified Ni catalysts. *J Catal* 2004;222:180–91.

632 <https://doi.org/10.1016/j.jcat.2003.10.022>.

633 [37] Iriondo A, Cambra JF, Barrio VL, Guemez MB, Arias PL, Sanchez-Sanchez MC,  
634 et al. Glycerol liquid phase conversion over monometallic and bimetallic catalysts:  
635 Effect of metal, support type and reaction temperatures. *Appl Catal B Environ*  
636 2011;106:83–93. <https://doi.org/10.1016/j.apcatb.2011.05.009>.

637 [38] Reynoso AJJ, Iriarte-Velasco U, Gutiérrez-Ortiz MAA, Ayastuy JLL. Highly  
638 stable Pt/CoAl<sub>2</sub>O<sub>4</sub> catalysts in Aqueous-Phase Reforming of glycerol. *Catal*  
639 *Today* 2020. <https://doi.org/10.1016/j.cattod.2020.03.039>.

640 [39] Zazo JA, Casas JA, Mohedano AF, Rodríguez JJ. Catalytic wet peroxide oxidation  
641 of phenol with a Fe/active carbon catalyst. *Appl Catal B Environ* 2006;65:261–8.  
642 <https://doi.org/10.1016/j.apcatb.2006.02.008>.

643 [40] Habte Lemji H, Eckstädt H. A pilot scale trickling filter with pebble gravel as  
644 media and its performance to remove chemical oxygen demand from synthetic  
645 brewery wastewater. *J Zhejiang Univ B (Biomedicine Biotechnol* 2013;14:924–  
646 33. <https://doi.org/10.1631/jzus.B1300057>.

647 [41] Oliveira ASS, Baeza JAA, Garcia D, Saenz de Miera B, Calvo L, Rodriguez JJJ,  
648 et al. Effect of basicity in the aqueous phase reforming of brewery wastewater for  
649 H<sub>2</sub> production. *Renew Energy* 2020;148:889–96.  
650 <https://doi.org/10.1016/J.RENENE.2019.10.173>.

651 [42] Oliveira AS, Cordero-Lanzac T, Baeza JA, Calvo L, Heras F, Rodriguez JJ, et al.  
652 Continuous aqueous phase reforming of a synthetic brewery wastewater with Pt/C  
653 and PtRe/C catalysts for biohydrogen production. *Chemosphere* 2021;281:130885.  
654 <https://doi.org/10.1016/j.chemosphere.2021.130885>.

655 [43] Zhang L, Karim AM, Engelhard MH, Wei Z, King DL, Wang Y. Correlation of  
656 Pt-Re surface properties with reaction pathways for the aqueous-phase reforming

657 of glycerol. *J Catal* 2012;287:37–43. <https://doi.org/10.1016/j.jcat.2011.11.015>.

658 [44] King DL, Zhang L, Xia G, Karim AM, Heldebrant DJ, Wang X, et al. Aqueous  
659 phase reforming of glycerol for hydrogen production over Pt-Re supported on  
660 carbon. *Appl Catal B Environ* 2010;99:206–13.  
661 <https://doi.org/10.1016/j.apcatb.2010.06.021>.

662 [45] Oliveira ASS, Aho A, Baeza JAA, Calvo L, Simakova ILL, Gilarranz MAA, et al.  
663 Enhanced H<sub>2</sub> production in the aqueous-phase reforming of maltose by feedstock  
664 pre-hydrogenation. *Appl Catal B Environ* 2021;281:119469.  
665 <https://doi.org/10.1016/j.apcatb.2020.119469>.

666 [46] Kim YY, Kim M, Jeong H, Kim YY, Choi SH, Ham HC, et al. High purity  
667 hydrogen production via aqueous phase reforming of xylose over small Pt  
668 nanoparticles on a  $\gamma$ -Al<sub>2</sub>O<sub>3</sub> support. *Int J Hydrogen Energy* 2020;45:13848–61.  
669 <https://doi.org/10.1016/j.ijhydene.2020.03.014>.

670 [47] Chen A, Chen P, Cao D, Lou H. Aqueous-phase reforming of the low-boiling  
671 fraction of bio-oil for hydrogen production: The size effect of Pt/Al<sub>2</sub>O<sub>3</sub>. *Int J*  
672 *Hydrogen Energy* 2015;40:14798–805.  
673 <https://doi.org/10.1016/j.ijhydene.2015.09.030>.

674 [48] Ciftci A, Michel DAJ, Hensen EJM. Influence of Pt particle size and Re addition  
675 by catalytic reduction on aqueous phase reforming of glycerol for carbon-  
676 supported Pt(Re) catalysts. *Appl Catal B Environ* 2015;174–175:126–35.  
677 <https://doi.org/10.1016/j.apcatb.2015.02.027>.

678 [49] Argyle M, Bartholomew C. Heterogeneous Catalyst Deactivation and  
679 Regeneration: A Review. *Catalysts* 2015;5:145–269.  
680 <https://doi.org/10.3390/catal5010145>.

681 [50] García-Gómez N, Valecillos J, Remiro A, Valle B, Bilbao J, Gayubo AG. Effect

of reaction conditions on the deactivation by coke of a NiAl<sub>2</sub>O<sub>4</sub> spinel derived catalyst in the steam reforming of bio-oil. *Appl Catal B Environ* 2021;297:120445. <https://doi.org/10.1016/J.APCATB.2021.120445>.

[51] Ciftci A, Ligthart DAJM, Sen AO, Van Hoof AJF, Friedrich H, Hensen EJM. Pt-Re synergy in aqueous-phase reforming of glycerol and the water-gas shift reaction. *J Catal* 2014;311:88–101. <https://doi.org/10.1016/j.jcat.2013.11.011>.

[52] Pipitone G, Zoppi G, Frattini A, Bocchini S, Pirone R, Bensaid S. Aqueous phase reforming of sugar-based biorefinery streams: from the simplicity of model compounds to the complexity of real feeds. *Catal Today* 2020;345:267–79. <https://doi.org/10.1016/j.cattod.2019.09.031>.

[53] Oliveira AS, Baeza JA, Calvo L, Alonso-Morales N, Heras F, Lemus J, et al. Exploration of the treatment of fish-canning industry effluents by aqueous-phase reforming using Pt/C catalysts. *Environ Sci Water Res Technol* 2018;4:1979–87. <https://doi.org/10.1039/c8ew00414e>.

[54] Falcone DD, Hack JH, Klyushin AY, Knop-gericke A, Schlo R, Davis RJ. Evidence for the bifunctional nature of Pt – Re catalysts for selective glycerol hydrogenolysis. *ACS Catal* 2015;5:5679–95. <https://doi.org/10.1021/acscatal.5b01371>.

